An effective method to model the combustion process in spark ignition engines

Abstract: Numerical simulation is a fundamental tool in the design and optimization procedure of an Internal Combustion (IC) engine; since combustion is the process that mostly influences the engine performance, efficiency and emissions, an effective combustion sub-model is fundamental. A simple, non-predictive, way to simulate the combustion evolution is to implement a mathematical function that reproduces the mass fraction burned (MFB) profile that is characterized by a sigmoidal trend; the most used, for this purpose, is the Wiebe function. In this paper the authors propose a different mathematical model, a Dose-Response (DR) type function, that shows some benefits when compared to Wiebe function, in particular a better interpolation of experimental MFB profiles in which the combustion extinction phase represents a large fraction of the whole combustion duration; this happens, for example, in Spark Ignition (SI) engines with a non-central location of the spark plug, which produces an asymmetric combustion propagation and in turn an asymmetric derivative of the experimental MFB profile. In this paper both the traditional Wiebe and the proposed DR function have been calibrated by means of experimental MFB profiles obtained from a supercharged SI engine fueled with natural gas; the two calibrated functions have been implemented in a zero-dimensional SI engine model and compared in terms of Indicated Mean Effective Pressure (IMEP) prediction reliability. The proposed DR function allowed both a better MFB profile interpolation and a better IMEP prediction for all the operating conditions tested (different engine speed and supercharging pressure), with a maximum prediction error of 2.1% compared with 2.9% of the Wiebe function.

Introduction

Computer simulations, in particular 0-D and 1-D thermodynamic models, are fundamental tools in the design and optimization process of IC engines [1] [2] [3]. All the processes involved in engine operation can be simulated: the flow through inlet and outlet ducts, the combustion process, the heat exchanged with combustion chamber walls and many others. Combustion is the process that mostly influences, with its development through the combustion chamber, both engine performance and pollutant emissions [4]. The combustion evolution depends on many factors: in-cylinder pressure and temperature, air/fuel ratio, turbulence intensity, fuel properties etc. Hence the combustion process is the most difficult to simulate due to its complexity. A wide variety of combustion models have been proposed in literature for 0-D and 1-D thermodynamic simulations, from the most complex and accurate predictive models, which require great computational efforts and allow reliable prediction of the performance attainable by the engine, to the simpler and easy to implement non-predictive models often employed for rough evaluations. The “two zones” combustion models [5] [6] [7] belong to the first category and refer to SI engines: in these models the mass inside the combustion chamber is divided in burnt and unburnt gas and the development of the flame front is modeled by evaluating the laminar and turbulent burning speed; this kind of models, after a proper calibration with experimental data, is able to predict the combustion evolution, and then the MFB curve, in different operating conditions (engine speed, load, air/fuel ratio etc.). An easier way to simulate the combustion evolution is to model the MFB profile using a mathematical function; the most used, for this purpose, is the well-known Wiebe function [8] reported in Equation *1*, that shows the typical sigmoidal trend of the experimental MFB profile as

function of crank angle. This method is not predictive because the pressure and temperature conditions of the gas is not taken into account, as well as all the other parameters affecting the flame front propagation (turbulence level, air-fuel ratio, residual gas dilution, etc..): once calibrated by means of experimental data, a single mathematical MFB profile is usually employed for all the engine operating conditions and then it will provide less accurate results compared to the previously described predictive methods. A double-Wiebe function can be used to simulate compression ignition engine combustion [9] and other kind of combustions such as HCCI [9] (homogeneous charge compression ignition), dual-fuel combustion [9] (diesel-Natural Gas) or gasoline-ethanol fuel blend combustion [10].

The following Equation 1 reports the Wiebe function.

$$x_{bw} = 1 - exp\left[-a\left(\frac{\vartheta-\vartheta_0}{\Delta\vartheta}\right)^{m+1}\right] \qquad 1$$

Where: x_{bw} is the mass fraction burned (MFB) according to Wiebe function, ϑ is the generic crank angle (CA) (after ignition), ϑ_0 is the spark ignition CA (the start of combustion), $\Delta\vartheta$ is the combustion duration (expressed in Crank Angle Degrees, CAD), a and m are the calibrating coefficients.

The authors of this paper in a previous work [13] collected several pressure curves from a supercharged SI engine, fueled with natural gas, and evaluated the experimental MFB curves by means of the Rassweiler-Withrow method [14]. As is clearly visible from the example of Figure 1, those curves exhibit a very large combustion extinction phase (MFB going from 80% to 100%) compared to the whole combustion duration and also an asymmetric MFB CA derivative dMFB/dϑ (the increasing part is different from the decreasing one). From the analysis of Figure 1, besides, it is evident that the best matching Wiebe function is not able to perfectly copy the asymmetric trend of the MFB derivative and the combustion extinction phase . The coefficients of the Wiebe function shown in Figure 1 are: a=13.7; m=2.18 and have been determined minimizing the root mean squared error (RMSE) between numeric and experimental data; the experimental MFB curve was obtained on a natural gas fueled spark ignition engine supercharged with a 1.2 bar Manifold Absolute Pressure (MAP) at 3500 rpm; the abscissa of the diagram reports the crank angle degrees (CAD) after start of combustion (ASOC).

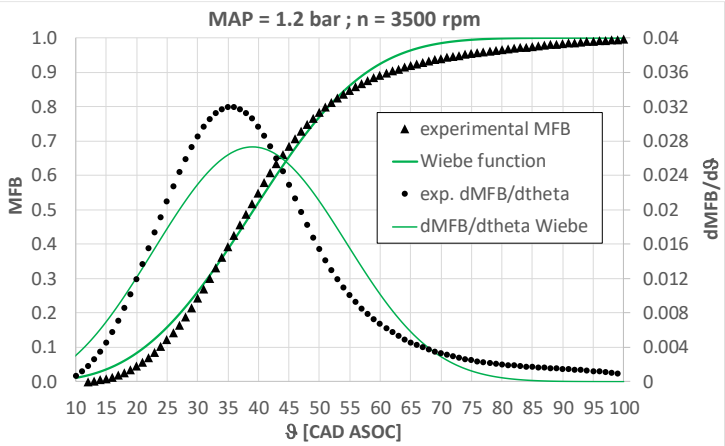

Figure 1 – Experimental MFB profile and its derivative interpolated with the best matching Wiebe function

It is possible to demonstrate, with simple numerical evaluations, that the shape of the MFB derivative and the combustion extinction duration are both related to the spark plug position in

the cylinder head; in particular, when the spark plug and the cylinder are not coaxial this produces an asymmetric combustion propagation (the flame front does not start in the cylinder axis and consequently does not reach all the combustion chamber lateral surfaces at the same time). The asymmetry of the flame front propagation produces an asymmetric MFB derivative profile and a prolonged combustion extinction phase. To prove this assumption a very simple numerical simulation has been carried out: with reference to the geometry of the SI engine described in [13], the combustion evolution has been simulated assimilating the flame front to a cylindrical surface centered in the spark plug position and whose radius starts from zero and grows with variable speed. A representation of the schematic flame front propagation is reported in Figure 2, where the non-central spark plug position is shown, and both piston and cylinder head have been modeled as flat surfaces. Figure 3 shows a picture of the engine head where the actual spark plug location is highlighted (17 mm from cylinder axis).

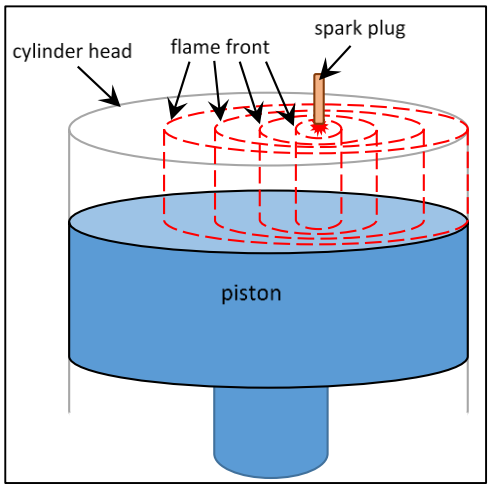

Figure 2 – Flame front development simplified model

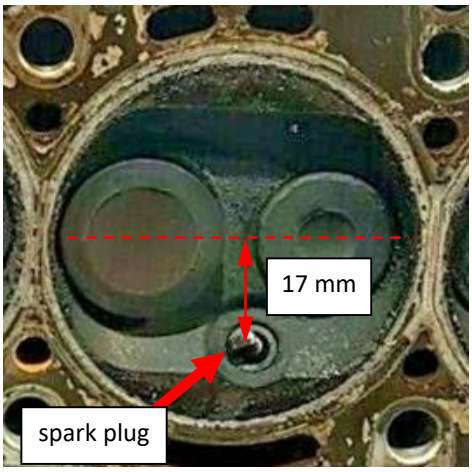

Figure 3 – Picture of the cylinder head where the actual spark plug position is shown

The speed variation of the cylinder radius, that represents the speed variation of the flame front, has been modeled with an increasing linear trend up to a maximum value followed by a decreasing linear trend down to zero (Figure 4): this reproduces, in a very simple way, the three combustion phases: combustion start, rapid combustion and combustion extinction; obviously the actual flame front speed depends on pressure, temperature and turbulence intensity on the combustion chamber so the linear trend is indeed an extreme over-simplification justified by the scope of this simulation. Knowing the combustion chamber radius, the experimental angular duration of the whole combustion (80 CAD), the engine speed and the spark plug position, it is possible to evaluate the mean flame front speed that allows the burned mass to completely fill the chamber volume (i.e. that allows the flame front to reach the farthest point of the combustion chamber); the two linear trends of the growing radius speed have been arranged to match the mean flame front speed previously evaluated. With the purpose to reproduce the experimental MFB, three different spark plug positions have been simulated: centered, 17 mm far from cylinder axis (the actual one) and 35 mm far from cylinder axis (almost tangent to the cylinder lateral surface). The three mentioned spark plug locations have been identified with three different symbols: Rc=0 mm (centered), Rb=17 mm (actual location) and Rw=35 mm (near cylinder wall). Figure 4 shows the three different flame front speed profiles, evaluated on the basis of the spark plug position, as function of the combustion crank angle ϑ, obviously if the spark plug is nearer to the chamber wall (Rw) the flame front needs a higher mean speed to reach the opposite wall in

the same time interval (the comparison was carried out with equal combustion duration), this is the reason for the three different speed profiles of Figure 4; the three linear trends are symmetric and the overall mean value of the flame speed is 12 m/s that is compatible with literature values [15]. The numeric MFB has been evaluated as the ratio between the volume of the growing cylinder and the volume of the whole combustion chamber, under the simplifying hypothesis of constant density. In Figure 5, Figure 6 and Figure 7 the comparison between numeric and experimental results are reported for the three assumed spark plug positions. From the qualitative analysis of these results it can be concluded that increasing the spark plug distance from cylinder axis produces both an increase of the combustion extinction phase and an asymmetric MFB derivative; moreover, the intermediate spark plug position (Rb=17 mm away from cylinder axis) produced the best matching with the experimental results confirming the reliability of the proposed simplified model. As already shown in Figure 1, the Wiebe function is not able to perfectly reproduce the MFB profile generated from the mentioned engine so the authors decided to explore other mathematical functions that are able to better reproduce the combustion extinction portion of the MFB profile and also an asymmetric MFB derivative.

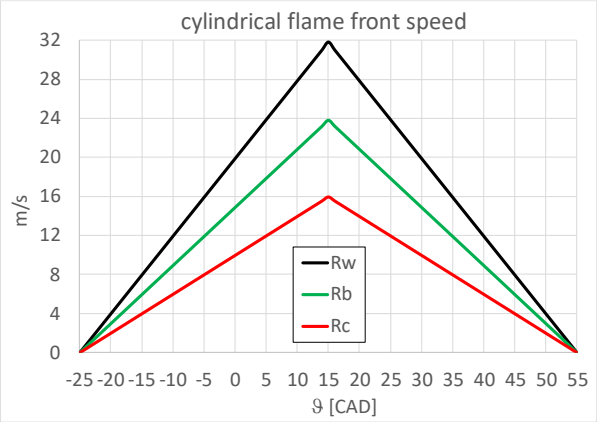

Figure 4 – Cylindrical flame front speed profiles for the three spark plug locations

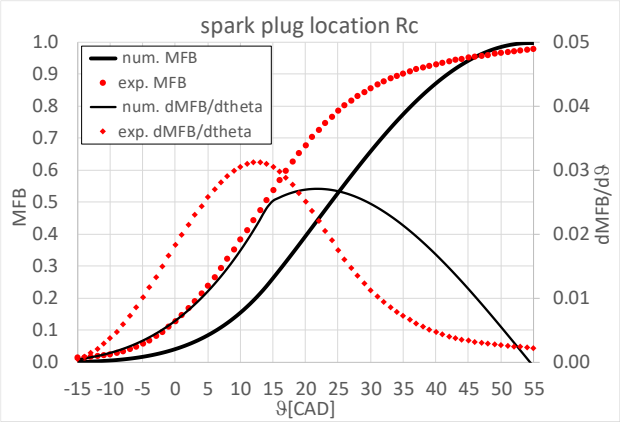

Figure 5 - Experimental and numeric MFB profile and its derivative with spark plug location Rc

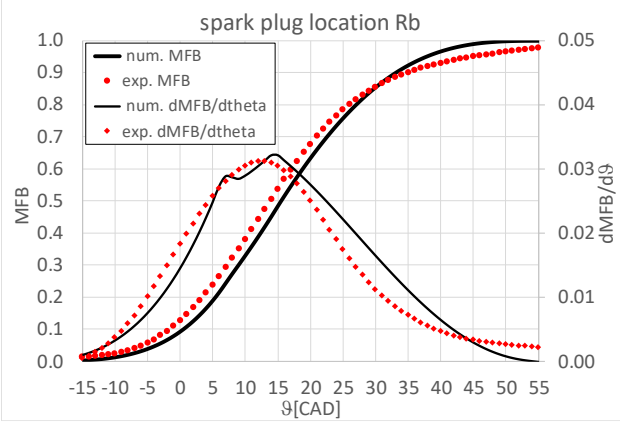

Figure 6 - Experimental and numeric MFB profile and its derivative with spark plug location Rb

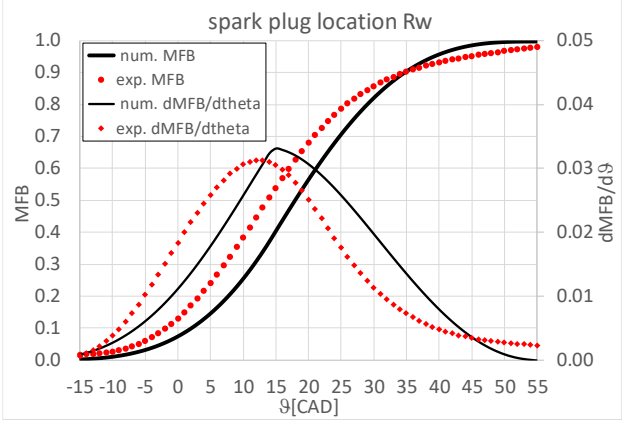

Figure 7 – Exp. and numeric MFB profile and its derivative with spark plug location Rw

The proposed model

In this paper the authors propose a different approach, with respect to the Wiebe function, to simulate the experimental MFB curve of a SI engine: a dose-response (DR) type function [11], in particular the Hill equation [12] (formerly used to quantify binding of oxygen to hemoglobin) displayed in Equation 2.

$$x_{bh} = \frac{(\vartheta-\vartheta_0)^n}{(\vartheta_{50}-\vartheta_0)^n+(\vartheta-\vartheta_0)^n} \qquad 2$$

Where: x_{bh} is the MFB according to Hill equation, ϑ_{50} is the CA that corresponds to 50% of the MFB (i.e. x_b=50%), (ϑ_{50} - ϑ_0) and n are the calibrating coefficients; to simplify it can be set ζ=(ϑ_{50} - ϑ_0). As already mentioned, the authors of this paper in a previous work [13] collected several pressure curves from a supercharged SI engine, fueled with natural gas, and evaluated the experimental MFB curves by means of the Rassweiler-Withrow method [14]; from subsequent analysis the authors found that the Hill equation better interpolates these MFB curves compared to Wiebe function. Figure 8 shows an example of experimental MFB profile interpolated with the best matching Wiebe and Hill equations (the coefficients of both equations where calibrated to minimize the root mean squared error (RMSE) between numeric and experimental data); it is evident the better interpolation of Hill equation in particular in the combustion extinction phase (MFB going from 80% to 100%). The Hill equation shows a better MFB curve interpolation thanks to its asymmetric derivative compared to the almost symmetric Wiebe function derivative. The coefficients of the Wiebe function shown in Figure 8 are: a=13.7; m=2.18; while the coefficients of the Hill equation are: ζ=38.2; n=4.69.

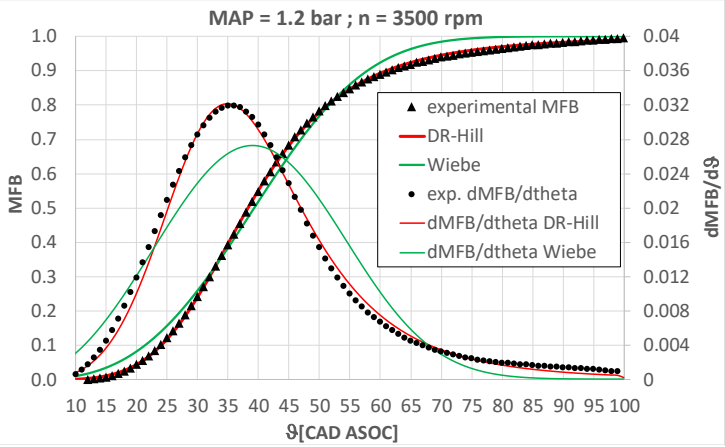

Figure 8 – Experimental MFB profile and its derivative interpolated with the best matching Wiebe and Hill functions

To highlight the better interpolation capability of Hill equation, compared to Wiebe function, a mathematic comparison between the two functions has been performed. The Hill and Wiebe coefficients, used in Figure 8, have been varied, in a reasonable range, in order to obtain different MFB curves. Figure 9 shows three different MFB curves, and its derivatives, obtained with the Hill equation for three different values of the coefficient ζ while the n coefficient is fixed at 4.7; it is quite evident the asymmetric trend of the derivative for all the displayed curves. Figure 10 shows three MFB curves, with the corresponding derivatives, obtained with the Wiebe function for three different values of the a coefficient while fixing the m coefficient at 2.2; in this case it is quite evident the almost symmetric trend of the derivative for all the curves. It can be concluded that the symmetry of the derivative is an intrinsic property of the Wiebe function as well as the asymmetric derivative is an intrinsic property of the Hill equation (at least in the range assumed by the functions coefficients in the present study) and this explains the better attitude of Hill equation to interpolate the experimental MFB curves generated by the tested engine.

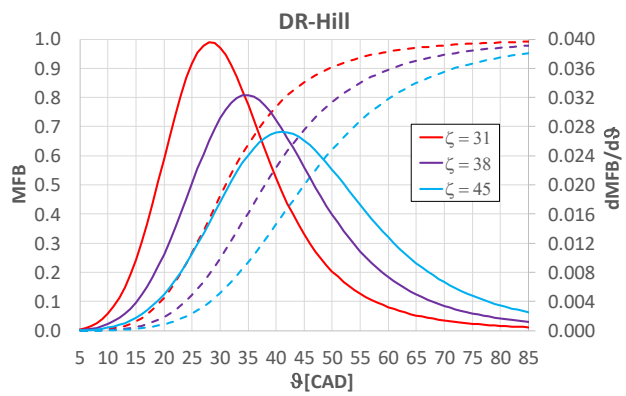

Figure 9 - DR-Hill MFB and its derivative (n=4.7)

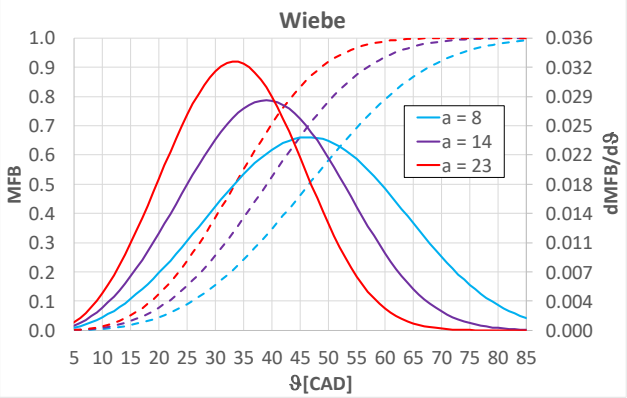

Figure 10 - Wiebe MFB and its derivative (m=2.2)

Main section

The aim of this work is to show the better interpolation capability of the Hill equation compared to Wiebe function in the case of an asymmetric MFB derivative profile that can be produced for example by a non-central spark plug position. For this purpose, some experimental MFB profiles have been used to calibrate the coefficients of both Wiebe and Hill functions, which have been implemented in a SI engine numerical simulation model to predict the indicated mean effective pressure (IMEP). The IMEP values obtained by simulation have been compared with the experimental measurements thus evaluating the prediction reliability of the two modeling functions. The experimental MFB profiles have been evaluated by means of the Rassweiler and Withrow method [14] applied on the pressure curves acquired in [13] for the different engine operating conditions reported in Table 1; Table 2 shows the specifications of the supercharged SI bi-fuel engine.

Table 1 - Operating conditions tested

Engine speed [rpm]	from 1500 to 5000 with steps of 500
MAP [bar]	1.0, 1.2, 1.4, 1.6
Inlet temperature [°C]	28±10
fuel	natural gas (85% Vol. Methane)
air/fuel ratio	Stoichiometric
Spark advance	maximum brake torque value

Table 2 – SI engine specifications

Number of cylinders	4
Displacement [cc]	1242
Bore [mm]	70.80
Stroke [mm]	78.86
Compression ratio	9.8
Rod to crank ratio	3.27
Intake valve/cylinder	1
Exhaust valve/cylinder	1
Gasoline injection system	PFI, Bosch EV6
NG injection system	PFI, Bosch EV1

To evaluate the interpolation capabilities of the Hill and Wiebe functions it is very useful, in the first place, to show some experimental MFB curves, obtained in different engine operating conditions, interpolated with the best matching Hill and Wiebe functions (i.e. calibrated with that specific MFB experimental curve). Figure 11, Figure 12, Figure 13 and Figure 14 show the experimental MFB curve and its derivative, interpolated with both functions, in four different operating conditions (low and high engine speed, low and high MAP). Table 3 reports the RMSE of the two functions, with respect to the whole experimental MFB curve, together with the absolute error evaluated in some specific points (MFB10, MFB50 and MFB90) and the calibrating parameters; it is

evident the better interpolation performance of the Hill equation that gives always a lower error (almost one order of magnitude) compared to the Wiebe function.

Table 3 – MFB prediction errors and calibrating parameters of the two functions

equation	engine speed [rpm]	MAP [bar]	RMSE	MFB10 abs. error	MFB50 abs. error	MFB90 abs. error	a	m	ζ	n
Wiebe	2000	1	0.032	0.044	0.030	0.046	10.2	1.87	-	-
Hill	2000	1	0.007	0.004	0.002	0.009	-	-	38.1	4.38
Wiebe	4500	1	0.029	0.040	0.033	0.040	15.2	2.53	-	-
Hill	4500	1	0.006	0.004	0.002	0.002	-	-	40.7	5.27
Wiebe	2000	1.6	0.035	0.042	0.031	0.053	18.8	2.00	-	-
Hill	2000	1.6	0.013	0.006	0.002	0.011	-	-	32.4	4.47
Wiebe	4500	1.6	0.025	0.032	0.023	0.032	15.2	2.36	-	-
Hill	4500	1.6	0.004	0.005	0.007	0.004	-	-	38.9	5.04

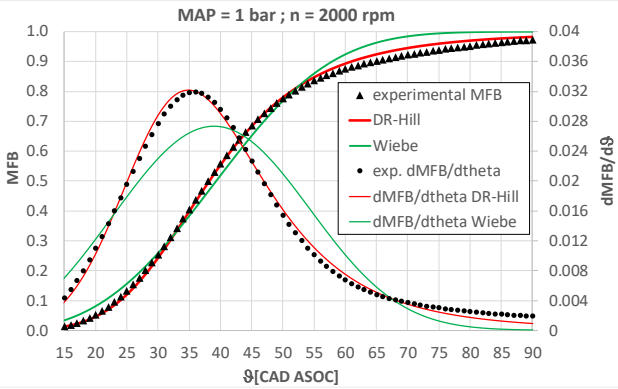

Figure 11 – Exp. MFB and derivative interpolated with the best matching functions (low MAP and low rpm)

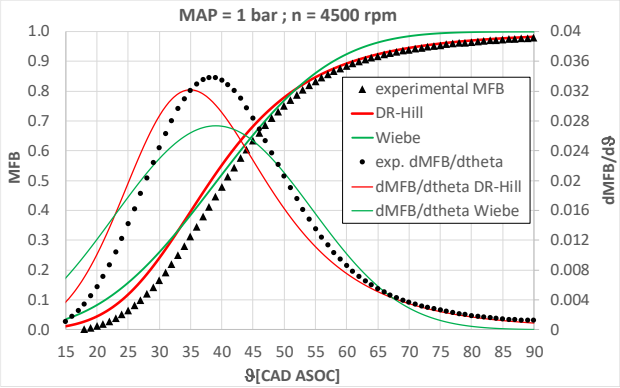

Figure 12 – Exp. MFB and derivative interpolated with the best matching functions (low MAP and high rpm)

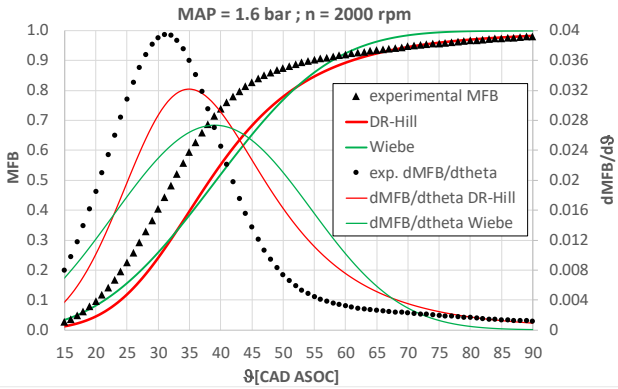

Figure 13 – Exp. MFB and derivative interpolated with the best matching functions (high MAP and low rpm)

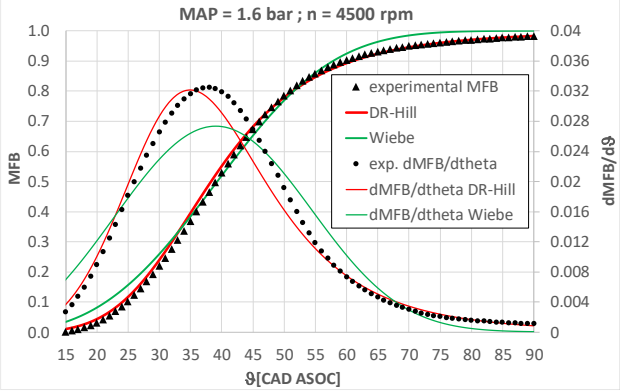

Figure 14 – Exp. MFB and derivative interpolated with the best matching functions (high MAP and high rpm)

For each of the 32 operating conditions reported in Table *1* the experimental MFB curve has been used to calibrate both the Wiebe and Hill functions by minimizing the RMSE between experimental and numerical values; the result is a set of calibration coefficients for each operating condition; since these are not predictive models, a unique value for each calibrating coefficient must be employed for all the engine operating conditions; to this purpose, an average value has been evaluated for each calibrating coefficient, as resumed in Table 4.

Table 4 – Average calibration coefficients

Function	equation	a	m	ζ	n
Wiebe	$x_b = 1 - exp\left[-a\left(\frac{\vartheta - \vartheta_0}{\Delta\vartheta}\right)^{m+1}\right]$	19.0	2.31	-	-
Hill	$x_b = \frac{(\vartheta - \vartheta_0)^n}{(\zeta)^n + (\vartheta - \vartheta_0)^n}$	-	-	36.9	4.78

The calibrated Wiebe and Hill functions (with the coefficients of Table 4) have been hence implemented in a zero-dimensional thermodynamic simulation model (whose description is reported in Appendix) employed to predict the pressure cycle of the supercharged SI engine, fueled with natural gas, and to provide the engine IMEP. Figure 15, Figure 16, Figure 17 and Figure 18 show the comparison, for different supercharging pressures, between the experimental IMEP and the values predicted by simulation using both Wiebe and Hill functions: it is quite evident the better prediction capability of the Hill equation compared to Wiebe function in particular at low MAP (1 bar and 1.2 bar); when MAP increases the prediction difference of the two functions tends to reduce.

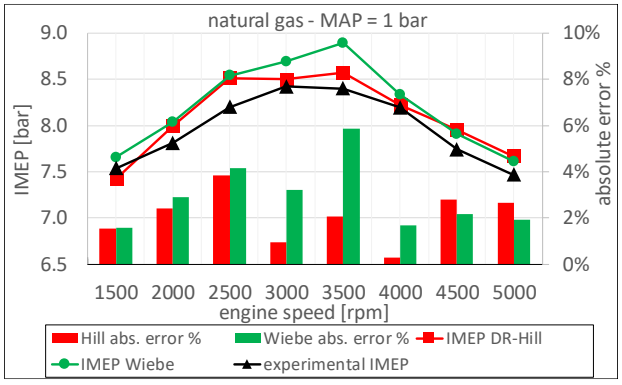

Figure 15 – Comparison between experimental and numerical IMEP (Wiebe and Hill) ; MAP = 1 bar; spark plug location Rb

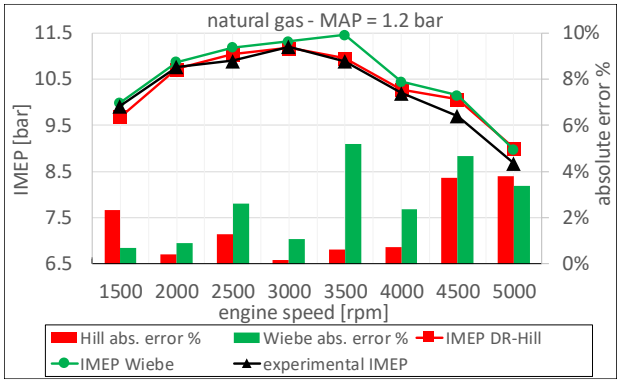

Figure 16 - Comparison between experimental and numerical IMEP (Wiebe and Hill) ; MAP = 1.2 bar; spark plug location Rb

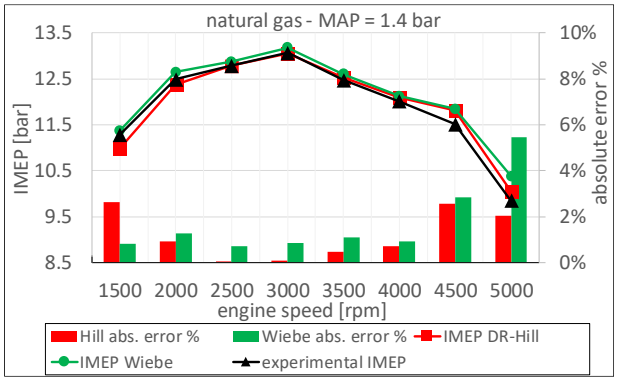

Figure 17 - Comparison between experimental and numerical IMEP (Wiebe and Hill) ; MAP = 1.4 bar; spark plug location Rb

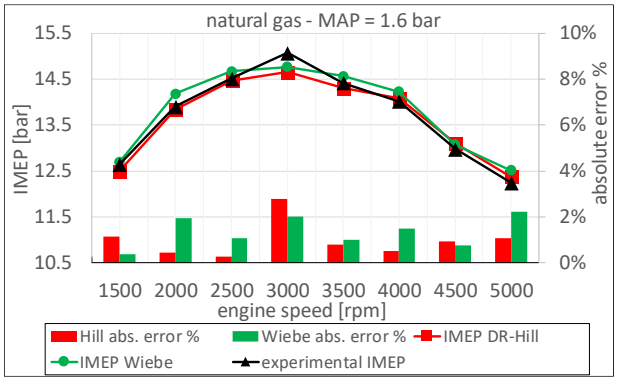

Figure 18 - Comparison between experimental and numerical IMEP (Wiebe and Hill) ; MAP = 1.6 bar; spark plug location Rb

Figure 15, Figure 16, Figure 17 and Figure 18 also report, as histograms, the absolute prediction error % of the numeric models compared to experimental data.

Table 5 – Numerical and experimental IMEP values for all the engine operating conditions

MAP=1 bar	engine speed [rpm]	spark advance [CAD BTDC]	engine IMEP [bar]	Hill IMEP [bar]	Wiebe IMEP [bar]	Hill abs. error %	Wiebe abs. error %
	1500	22	7.54	7.42	7.66	1.5	1.6
	2000	25	7.81	8.00	8.04	2.4	2.9
	2500	27	8.20	8.51	8.54	3.8	4.2
	3000	28	8.42	8.50	8.69	0.9	3.2
	3500	29	8.40	8.57	8.89	2.0	5.9
	4000	28	8.20	8.22	8.33	0.3	1.7
	4500	30	7.74	7.96	7.91	2.8	2.2
	5000	31	7.47	7.67	7.61	2.7	1.9
					mean value	**2.1**	**2.9**
MAP=1.2 bar	engine speed [rpm]	spark advance [CAD BTDC]	engine IMEP [bar]	Hill IMEP [bar]	Wiebe IMEP [bar]	Hill abs. error %	Wiebe abs. error %
	1500	21	9.92	9.69	9.99	2.3	0.7
	2000	23	10.77	10.73	10.87	0.4	0.9
	2500	24	10.90	11.04	11.19	1.3	2.6
	3000	25	11.20	11.18	11.32	0.2	1.1
	3500	26	10.89	10.96	11.46	0.6	5.2
	4000	27	10.20	10.28	10.44	0.7	2.4
	4500	29	9.70	10.06	10.15	3.7	4.7
	5000	30	8.68	9.01	8.98	3.8	3.4
					mean value	**1.6**	**2.6**
MAP=1.4 bar	engine speed [rpm]	spark advance [CAD BTDC]	engine IMEP [bar]	Hill IMEP [bar]	Wiebe IMEP [bar]	Hill abs. error %	Wiebe abs. error %
	1500	20	11.28	10.99	11.37	2.6	0.8
	2000	22	12.49	12.37	12.65	0.9	1.3
	2500	24	12.78	12.79	12.88	0.0	0.7
	3000	24	13.07	13.06	13.18	0.1	0.9
	3500	25	12.47	12.53	12.61	0.4	1.1
	4000	27	12.01	12.09	12.12	0.7	0.9
	4500	28	11.51	11.81	11.84	2.6	2.8
	5000	29	9.85	10.04	10.38	2.0	5.4
					mean value	**1.2**	**1.7**
MAP=1.6 bar	engine speed [rpm]	spark advance [CAD BTDC]	engine IMEP [bar]	Hill IMEP [bar]	Wiebe IMEP [bar]	Hill abs. error %	Wiebe abs. error %
	1500	20	12.65	12.50	12.70	1.2	0.4
	2000	22	13.91	13.84	14.18	0.5	2.0
	2500	23	14.51	14.47	14.67	0.3	1.1
	3000	24	15.07	14.65	14.77	2.8	2.0
	3500	25	14.42	14.31	14.56	0.8	1.0
	4000	25	14.02	14.09	14.23	0.5	1.5
	4500	27	12.98	13.10	13.07	0.9	0.7
	5000	28	12.24	12.38	12.51	1.1	2.2
					mean value	**1.0**	**1.4**

In Table 5 all the experimental and numerical IMEP are reported together with the absolute percentage prediction error of both combustion models; the model based on Hill equation reveals more accurate (on average) than the one based on Wiebe function for all the supercharging pressures tested. The maximum IMEP prediction error is obtained in the case of naturally aspirated engine (MAP=1 bar); in this case, the Hill equation gives an average absolute error of 2.1% while using the Wiebe function an average absolute error of 2.9 % is obtained; for MAP=1.2 bar the mean abs. error using the Hill equation is 1.6% while using the Wiebe function it is 2.6%; increasing MAP reduces the errors obtained by both models.

Figure 19 shows the comparison between numeric and experimental pressure curves obtained in the same engine operating conditions reported in Figure 8; this confirms that the best matching Hill function (i.e. calibrated with a specific MFB experimental profile) provides, for that specific

operating condition, a better pressure data prediction compared to the best matching Wiebe function; moreover the Hill equation, calibrated with a wide set of MFB profiles, provides a better IMEP prediction compared to Wiebe function in all the tested operating conditions (from Figure 15 to Figure 18) and also a better interpolation of the pressure curve as can be seen in Figure 20.

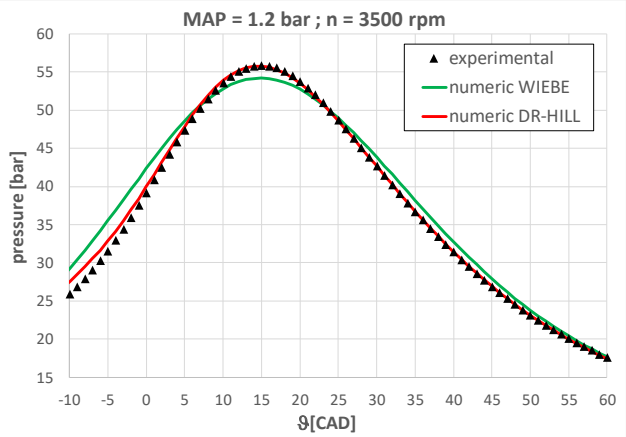

Figure 19 – Experimental and simulated pressure curves (with the best matching Wiebe and Hill equations)

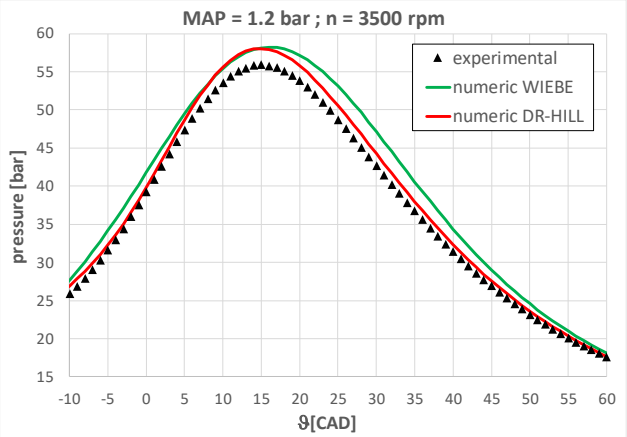

Figure 20 – Experimental and simulated pressure curves (with the average calibration coefficients of the Wiebe and Hill equations)

Conclusions

This paper focuses on simple modelling of the heat released by combustion in spark ignition engines. The mostly adopted approach for non-predictive 0-D and 1-D thermodynamic simulations is the Wiebe function, usually preferred for its simplicity and ease of implementation when a great level of accuracy and reliability is not required by the simulations performed. The analysis of the results obtained by several experimental tests however revealed that the Wiebe function is not adequate for describing the heat released by combustion ignited by a non-central spark plug: in these cases, in effect, the sigmoidal heat released curve reveal a slow extinction phase, which is not easily represented by the use of the Wiebe function. The authors found a solution to this problem using a different mathematical formulation, known as DR-Hill function, whose asymmetric derivative proved to better interpolate the experimental curves obtained from an engine with a non-central position of the spark plug. The Hill equation shows an MFB prediction error about one order of magnitude lower than the Wiebe function in specific points of the MFB curve (MFB10, MFB50 and MFB90) and also considering the RMS error evaluated over the whole MFB curve.

The better MFB curve interpolation produces a better combustion heat release prediction, when the equation is implemented in a zero-dimensional simulation, and in turn a better engine IMEP prediction as is widely shown in this paper; the average prediction error obtained using the Hill equation, in the worst case, is 2.1% while using the Wiebe function it is 2.9% (MAP=1 bar); for MAP=1.2 bar, the Hill average error is 1.6% compared to the 2.6% of the Wiebe function; a further increase of MAP reduces the error of both models. A further investigation involving experimental MFB profiles coming from different engines could confirm the better prediction capabilities of the Hill equation compared to Wiebe function maybe also in the case of MFB profiles with symmetric derivative.

Appendix

The previously mentioned SI engine has been simulated by a numerical model, that will be described in this paragraph, in order to provide pressure cycles to be compared with the experimental ones. The cylinder has been simulated as a zero-dimensional capacity characterized by variable volume, variable mass and energy exchanges with the environment. A scheme of the cylinder model is reported in Figure 21 where: p, T, v and V are the gas pressure [bar] , temperature [K] specific volume [m^3/kg] and volume [m^3] inside the cylinder; $\dot{m}_{in}, \dot{m}_{out}$ *and* $\dot{m}_l$ [kg/s] are the mass flow entering into the cylinder, the mass flow leaving the cylinder and the gas leaks respectively; $Q_{comb.}$ [J] is the heat released during combustion and Q_{ht} [J] is the heat exchanged with cylinder walls.

The generic volume inside the cylinder is a function of CA: V=V(ϑ); it depends also on rod to crank ratio and volumetric compression ratio.

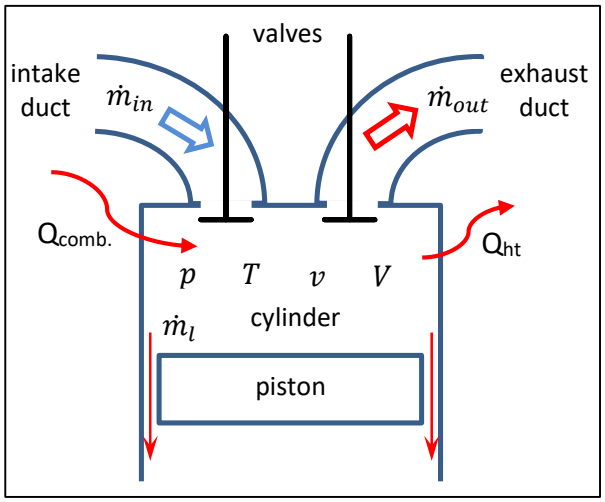

Figure 21 – Cylinder model

Applying to the cylinder the first law of thermodynamic for open systems in differential form:

$$dQ + dL + dm_{in}h^0_{in} - dm_{out}h^0_{out} - dm_l h = dU \qquad 3$$

where dU [J] is the system internal energy variation during a time interval dt [s]; Q [J] is the total heat provided to the system and L [J] is the piston work; h^0_{in} and h^0_{out} [J/kg] are the stagnation enthalpies of the incoming fluid dm_{in} and outgoing fluid dm_{out} [kg] respectively; h [J/kg] is the enthalpy of the fluid inside the cylinder (that corresponds to h^0_{out}) and dm_l [kg] are the leaks.

The piston work depends on volume variation hence

$$dL = -pdV \;\Rightarrow\; dQ + dm_{in}h^0_{in} - dm_{out}h^0_{out} - dm_l h = dU + pdV$$

and introducing the enthalpy H [J]

$$dU = d(H - pV) = dH - pdV - Vdp \;\Rightarrow dU + pdV = dH - Vdp$$

then

$$dQ + dm_{in}h^0_{in} - dm_{out}h^0_{out} - dm_l h = dH - Vdp \qquad 4$$

assuming, to simplify, that there is only air inside the cylinder and considering it as an ideal gas, the perfect gas law can be written as follows

$$pV = mRT \quad R = c_p - c_v \quad k = \frac{c_p}{c_v} \Rightarrow c_p = \frac{k}{k-1}R$$

where m [kg] is the air mass inside the cylinder, R=287.1 [J/(kg K)] is the air constant, c_p and c_v [J/(kg K)] are the specific heat at constant pressure and constant volume respectively and k is the isentropic equation exponent; the c_p has been evaluated by means of the polynomial expression reported on the JANAF tables [16].

Using the perfect gas law and remembering that for an ideal gas the enthalpy variation depends on temperature variation through c_p

$$dH = c_p d(mT) = c_p d\left(\frac{pV}{R}\right) \Rightarrow dH = \frac{c_p}{R} d(pV) = \frac{k}{k-1}(pdV + Vdp)$$

substituting this expression of *dH* in 4

$$dQ + dm_{in}h_{in}^0 - dm_{out}h_{out}^0 - dm_l h = \frac{k}{k-1}(pdV + Vdp) - Vdp$$

$$dQ + dm_{in}h_{in}^0 - dm_{out}h_{out}^0 - dm_l h = \frac{k}{k-1}pdV + \frac{1}{k-1}Vdp$$

dividing by *dt* and remembering that $h=h^0_{out}$ the differential equation of the pressure inside the cylinder is obtained

$$\frac{dp}{dt} = \frac{k-1}{V}\frac{dQ}{dt} - \frac{k \cdot p}{V}\frac{dV}{dt} + \frac{k-1}{V}[\dot{m}_{in}h_{in}^0 - h(\dot{m}_{out} + \dot{m}_l)] \qquad 5$$

integrating Equation 5, between the initial simulation time t_0 [s] and the generic time t [s], the cylinder pressure p [bar] can be obtained

$$p = MAP + \int_{t_0}^{t} \frac{dp}{dt} dt$$

the mass of air inside the cylinder can be evaluated by the following integral

$$m = m_0 + \int_{t_0}^{t} (\dot{m}_{in} - \dot{m}_{out} - \dot{m}_l) dt \qquad 6$$

$$m_0 = \frac{V_{TDC}}{v_0}$$

where m_0 is the mass at time t_0, v_0 the corresponding specific volume and V_{TDC} is the cylinder volume at top dead center (TDC).

The gas leaks has been modeled as a chocked flow through a convergent nozzle with a throat section $A_{th} = \pi \cdot D \cdot l$ where D [mm] is the piston diameter and l [mm] is the gap between piston and cylinder, the gas leaks mass flow is then

$$\dot{m}_l = A_{th}\sqrt{p \cdot \varrho \cdot k\left(\frac{2}{k+1}\right)^{\frac{k+1}{k-1}}}$$

for what concern the heat flux it can be divided in two terms: the heat developed during combustion and the heat exchanged with combustion chamber walls as reported below

$$\frac{dQ}{dt} = \frac{dQ_{comb.} - dQ_{ht}}{dt}$$

the combustion heat flux is

$$\frac{dQ_{comb.}}{dt} = \frac{\omega \cdot dQ_{comb.}}{d\vartheta} = \omega \cdot H_i \cdot m_f \frac{dx_b}{d\vartheta}$$

where ω [rad/s] is the engine angular speed, H_i [J/kg] is the fuel lower heating value, m_f is the fuel mass inside the cylinder at inlet valve closure (IVC) and x_b is the burned mass fraction that can be modeled by means of Equation *1* or Equation *2*. To take into account the engine volumetric efficiency penalization produced by natural gas the following formula has been used to evaluate the fuel mass m_f

$$m_f = \frac{m_{IVC}}{\alpha + \frac{\delta_a}{\delta_f}}$$

where m_{IVC} is the mass, evaluated by Equation 6, at IVC, α is the air/fuel ratio, δ_a and δ_f are the air and fuel densities respectively.

the heat exchanged between fluid and combustion chamber walls is evaluated by

$$\frac{dQ_{ht}}{dt} = h'S(T - T_w)$$

where $T_w = \text{wall temperature}; h' = \text{convective coefficient}; S = \text{combustion chamber surface}$

$$S = 2 \cdot \frac{\pi D^2}{4} + \pi D \cdot \frac{V}{\frac{\pi D^2}{4}}$$

the convective heat transfer coefficient is evaluated by means of the Woschni model [17]

$$h = F_w D^{-0.2} \cdot p^{0.8} \cdot C_w^{0.8} \cdot T^{-0.55}$$

where F_w is a calibration coefficient and C_w is the average gas velocity evaluated by

$$C_w = \left[C_1 v_p + C_2 \frac{V' T_{IVC}}{p_{IVC} V_{IVC}} (p - p_m) \right]$$

where

$v_p = mean\ piston\ speed;\ C_1 = 6.18\ during\ intake\ and\ exhaust, 2.28\ otherwise$

$C_2 = 0\ during\ intake, compression\ and\ exhaus, 3.24 \cdot 10^{-3}\ \left[\frac{m}{s \cdot K}\right] during\ combustion\ and\ expansion$

T_{IVC}, p_{IVC} and V_{IVC} refer to the gas temperature, pressure and volume at IVC,

p_m is the motored pressure (without combustion) and V' is the engine displacement

The inlet and exhaust ducts and the inlet and outlet manifolds have been simulated with a lumped parameters approach, all the mentioned elements are zero-dimensional and have some local properties associated both with inertia (mass of the fluid) and with capacity (volume).

The scheme of the inlet and outlet systems are shown in Figure 22.

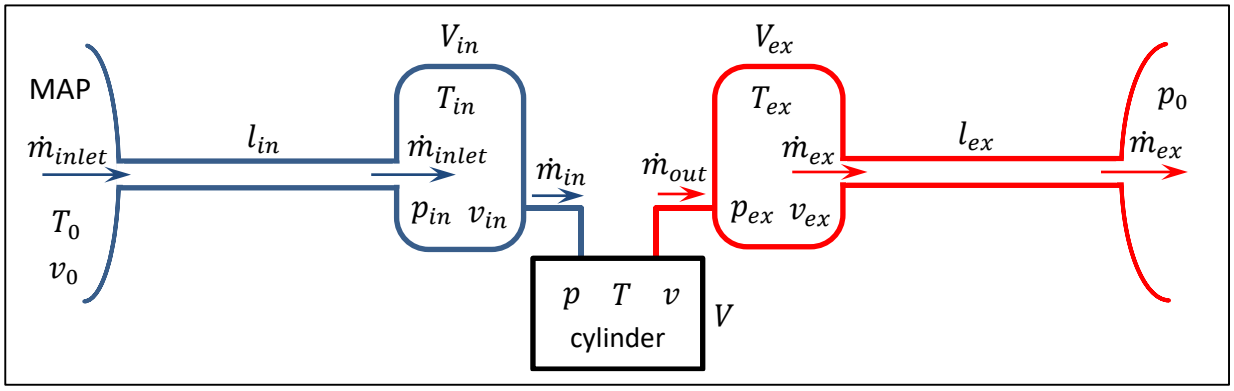

Figure 22 – Inlet and outlet systems

The inlet and outlet ducts are represented with elements having both inertia and capacity properties while the manifolds have only capacity property. The inertia element is characterized by the same mass flow at both sides, such as an incompressible fluid, and the mass inside the element is accelerated by the pressure difference at the element sides; the capacity element, on the contrary, is able to collect mass from the difference between ingoing and outgoing mass flow integrated over time while the pressure at both sides of the element is the same. The geometric parameter characterizing an inertia element is the length while for a capacity element it is the volume.

With reference to the inlet portion of the system displayed in Figure 22 one can write the equilibrium of the inertia element (which length is l_{in}) subject to the following forces: the MAP on the left surface, p_{in} on the right surface and the friction force on the lateral surface that contrast the motion of the fluid

$$(MAP - p_{in} - \mu\dot{m}_{inlet}^2)S_{in\,max} = m \cdot a = m\frac{dc}{dt} \qquad 7$$

$$S_{in\,max} = \frac{\pi D_{V\,in}^2}{4}$$

where p_{in} is the pressure inside the capacity element, μ is a friction coefficient, $\dot{m}_{inlet}$ is the mass flow through the element, c and a are the velocity and acceleration of the mass m inside the element and D_{vin} is the inlet valve seat diameter; the simplifying assumption is that the inlet duct cross section area corresponds to the inlet valve seat area that, in turn, equals the fully lifted valve curtain area ($S_{in\,max}$) neglecting the valve stem. From Equation 7 it follows that

$$\dot{m}_{inlet} = \frac{c \cdot S_{in\,max}}{v_0} \Rightarrow c = \frac{\dot{m}_{inlet} \cdot v_0}{S_{in\,max}} \Rightarrow m\frac{dc}{dt} = \frac{m \cdot v_0}{S_{in\,max}}\frac{d\dot{m}_{inlet}}{dt} = l_{in}\frac{d\dot{m}_{inlet}}{dt}$$

where v_0 is the specific volume in the inlet manifold. With reference to the inlet capacity element

$$\frac{dm_{in}}{dt} = \dot{m}_{inlet} - \dot{m}_{in} \qquad m_{in} = \frac{V_{in}}{v_0} + \int_{t_0}^{t}\frac{dm_{in}}{dt}dt \qquad v_{in} = \frac{V_{in}}{m_{in}}$$

where $\dot{m}_{in}$ is the mass flow going from the capacity element to the engine trough the inlet valve, m_{in} is the mass inside the capacity element, V_{in} and v_{in} the volume and specific volume of the element respectively and V_{in}/v_0 is the initial mass inside the element.

Applying the first law to the capacity element one can find the differential equation of the pressure inside the element p_{in}

$$\frac{dp_{in}}{dt} = \frac{k-1}{V_{in}}\left(\dot{m}_{inlet} \cdot c_p T_0 - \dot{m}_{in} \cdot c_p T_{in}\right) \qquad p_{in} = MAP + \int_{t_0}^{t}\frac{dp_{in}}{dt}dt \qquad T_{in} = \frac{p_{in} \cdot v_{in}}{R}$$

to find the mass flow $\dot{m}_{in}$ the engine inlet valve has been modelled as a convergent nozzle with throat section S_{in}, that is the current valve curtain area; here two equations are reported, one for the subsonic flow and one for the chocked flow together with the chocked flow condition

$$\dot{m}_{in} = \begin{cases} S_{in} \cdot \sqrt{\frac{p_{in}}{v_{in}} \cdot \frac{2k}{k-1}\left[\left(\frac{p}{p_{in}}\right)^{\frac{2}{k}} - \left(\frac{p}{p_{in}}\right)^{\frac{k+1}{k}}\right]}, & \left(\frac{p}{p_{in}}\right) > \left(\frac{2}{k+1}\right)^{\frac{k}{k-1}} \\ S_{in} \cdot \sqrt{\frac{p_{in}}{v_{in}} \cdot k\left(\frac{2}{k+1}\right)^{\frac{k+1}{k-1}}}, & \left(\frac{p}{p_{in}}\right) \le \left(\frac{2}{k+1}\right)^{\frac{k}{k-1}} \end{cases} \qquad S_{in} = L_{in} \cdot S_{in\,max}$$

$$L_{in} = \frac{inlet\ valve\ current\ lift}{inlet\ valve\ maximum\ lift}$$

With reference to the outlet portion of the system displayed in Figure 22, as well as previously described for the inlet portion, it can be written:

$$(p_{ex} - p_0 - \mu\dot{m}_{ex}^2)S_{ex\,max} = m' \cdot a' = m'\frac{dc'}{dt} \qquad S_{ex\,max} = \frac{\pi D_{V\,ex}^2}{4}$$

$$\dot{m}_{ex} = \frac{c' \cdot S_{ex\,max}}{v_{ex}} \;\Rightarrow\; c' = \frac{\dot{m}_{ex} \cdot v_{ex}}{S_{ex\,max}} \;\Rightarrow\; m'\frac{dc'}{dt} = \frac{m' \cdot v_{ex}}{S_{ex\,max}}\frac{d\dot{m}_{ex}}{dt} = l_{ex}\frac{d\dot{m}_{ex}}{dt}$$

$$\frac{d\dot{m}_{ex}}{dt} = \frac{(p_{ex} - p_0 - \mu\dot{m}_{ex}^2)S_{ex\,max}}{l_{ex}} \;\Rightarrow\; \dot{m}_{ex} = \int_{t_0}^{t} \frac{(p_{ex} - p_0 - \mu\dot{m}_{ex}^2)S_{ex\,max}}{l_{ex}}dt$$

$$\frac{dm_{ex}}{dt} = \dot{m}_{out} - \dot{m}_{ex} \qquad m_{ex} = \frac{V_{ex}}{v_0} + \int_{t_0}^{t}\frac{dm_{ex}}{dt}dt \qquad v_{ex} = \frac{V_{ex}}{m_{ex}}$$

$$\frac{dp_{ex}}{dt} = \frac{k-1}{V_{ex}}\left(\dot{m}_{out} \cdot c_p T - \dot{m}_{ex} \cdot c_p T_{ex}\right) \qquad p_{ex} = p_0 + \int_{t_0}^{t}\frac{dp_{ex}}{dt}dt \qquad T_{ex} = \frac{p_{ex} \cdot v_{ex}}{R}$$

$$\dot{m}_{out} = \begin{cases} S_{ex} \cdot \sqrt{\frac{p}{v} \cdot \frac{2k}{k-1}\left[\left(\frac{p_{ex}}{p}\right)^{\frac{2}{k}} - \left(\frac{p_{ex}}{p}\right)^{\frac{k+1}{k}}\right]}, & \left(\frac{p_{ex}}{p}\right) > \left(\frac{2}{k+1}\right)^{\frac{k}{k-1}} \\ S_{ex} \cdot \sqrt{\frac{p}{v} \cdot k\left(\frac{2}{k+1}\right)^{\frac{k+1}{k-1}}}, & \left(\frac{p_{ex}}{p}\right) \le \left(\frac{2}{k+1}\right)^{\frac{k}{k-1}} \end{cases} \qquad S_{ex} = L_{ex} \cdot S_{ex\,max}$$

$$L_{ex} = \frac{exhaust\ valve\ current\ lift}{exhaust\ valve\ maximum\ lift}$$

the superscript ‘ refers to the variables in the outlet duct.

All the model calibration parameters have been found either by direct measurements or by comparison with experimental data.

All the previously mentioned equations have been implemented in LabVIEW Control Design and Simulation Module and solved by means of a Runge-Kutta 23 ODE solver (A variable step-size solver that starts with a third order method and embeds a set of Bogacki-Shampine coefficients for a second order method [18]).

Figure 23, Figure 24, Figure 25 and Figure 26 show examples of the simulated pressure curve compared with the experimental one; the operating condition is: engine speed=4000 rpm and MAP=1.6 bar; the fuel is natural gas.

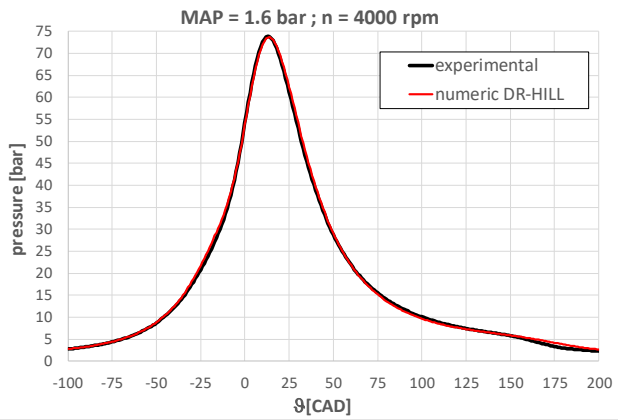

Figure 23 – Simulated and experimental pressure vs. ϑ; the fuel is natural gas

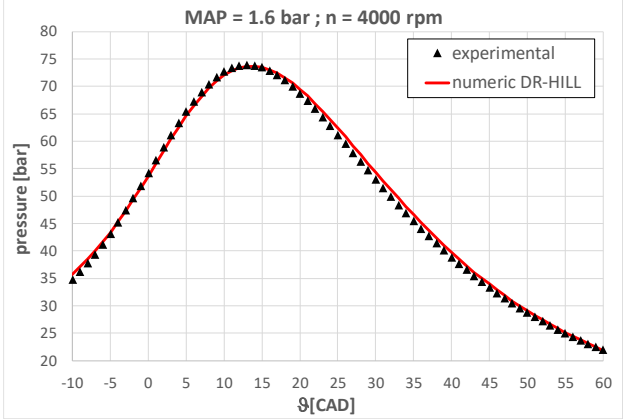

Figure 24 – A detail of the combustion zone

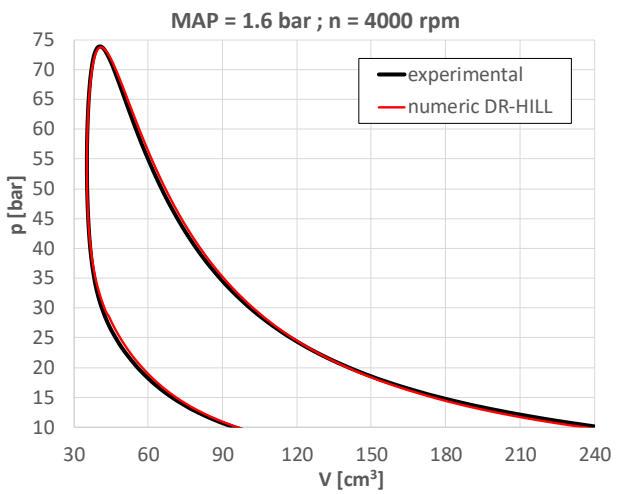

Figure 25 – Pressure vs. volume curves; the fuel is natural gas

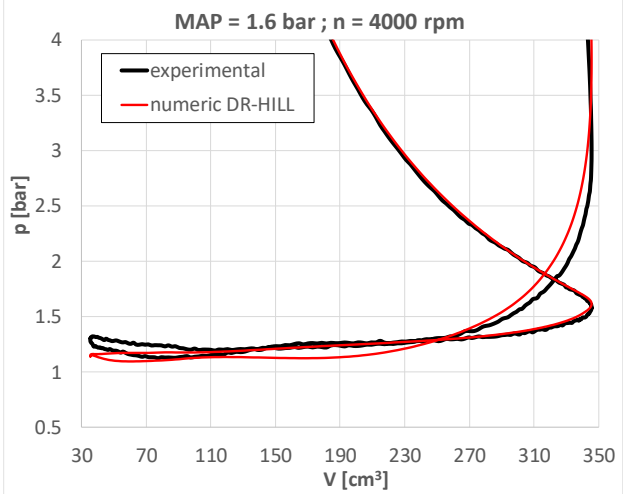

Figure 26 – A detail of the intake and exhaust phases

Symbols and abbreviations

0-D = zero dimensional
1-D = mono dimensional
a, m = Wiebe function calibrating coefficients
ASOC = after start of combustion
A_{th} = throat section
CAD = Crank Angle Degrees
c_p; c_v = specific heat at constant pressure and constant volume respectively
C_w = average gas velocity
D = piston diameter
dm_{in} = incoming fluid
dm_l = gas leaks
dm_{out} = outgoing fluid
DR = Dose Response
dt = simulation time step
dU = internal energy variation
D_{vex} = exhaust valve seat diameter
D_{vin} = inlet valve seat diameter
F_w C_1 and C_2= heat transfer calibration coefficients
H = enthalpy of the fluid inside the cylinder
h = specific enthalpy of the fluid inside the cylinder
h' = convective heat transfer coefficient

h^0_{in} = stagnation specific enthalpy of the incoming fluid
h^0_{out} = stagnation specific enthalpy of the outgoing fluid
HCCI = homogeneous charge compression ignition
H_i = fuel lower heating value
IC = Internal Combustion
IMEP = Indicated Mean Effective Pressure
IVC = inlet valve closure
k = isentropic exponent
l = gap between piston and cylinder
L = piston work
l_{ex} = exhaust duct length
L_{ex} = ratio between the exhaust valve current lift and the maximum lift
l_{in} = inlet duct length
L_{in} = ratio between the inlet valve current lift and the maximum lift
$\dot{m}_{ex}$ = mass flow exiting the exhaust capacity element
$\dot{m}_{in}$ = mass flow entering into the cylinder
$\dot{m}_{inlet}$ = mass flow entering the inlet capacity element
$\dot{m}_l$ = gas leaks
$\dot{m}_{out}$ = mass flow leaving the cylinder
m_0 = mass inside the cylinder at time t_0
MAP = Manifold Absolute Pressure
m_{ex} = mass inside the exhaust capacity element
m_f = fuel mass inside the cylinder at IVC
MFB = Mass Fraction Burned
MFB10; MFB50; MFB90 = MFB values corresponding to 10%, 50% and 90% respectively
m_{in} = mass inside the inlet capacity element
m_{IVC} = air mass inside the cylinder at IVC
ODE = Ordinary Differential Equation
p = simulated gas pressure
p_{ex} = pressure inside the exhaust capacity element
PFI = Port Fuel Injection
p_{in} = pressure inside the inlet capacity element
p_m = motored pressure (without combustion)
Q = total heat provided to the system
$Q_{comb.}$ = heat released during combustion
Q_{ht} = heat exchanged with cylinder walls
R = perfect gas law constant
Rb = spark plug location between cylinder axis and wall
Rc = centered spark plug location
RMSE = Root Mean Squared Error
rpm = rounds per minute
Rw = spark plug location near cylinder wall
S = combustion chamber surface
S_{ex} = exhaust valve curtain area
$S_{ex\ max}$ = fully lifted exhaust valve curtain area
SI = Spark Ignition
S_{in} = inlet valve curtain area
$S_{in\ max}$ = fully lifted inlet valve curtain area
t = generic simulation time
T = simulated gas temperature
t_0 = simulation starting time
TDC = Top Dead Center

T_{ex} = temperature inside the exhaust capacity element
T_{in} = temperature inside the inlet capacity element
T_{IVC}, p_{IVC} and V_{IVC} = gas temperature, pressure and volume at IVC
T_w = wall temperature
V = generic cylinder volume
v = simulated gas specific volume
V' = engine displacement
v_0 = specific volume at time t_0
V_{ex} and v_{ex} = volume and specific volume of the exhaust capacity element respectively
V_{in} and v_{in} = volume and specific volume of the inlet capacity element respectively
v_p = mean piston speed
V_{TDC} = cylinder volume at TDC
x_b = burned mass fraction
x_{bh} = MFB according to Hill equation
x_{bw} = MFB according to Wiebe function

$\Delta\vartheta$ = combustion arc (angular duration)
ϑ = generic crank angle
ϑ_0 = spark ignition crank angle
ϑ_{50} = the CA that corresponds to 50% of the MFB
α = air/fuel ratio
δ_a; δ_f = air and fuel densities respectively
μ = friction coefficient
ω = engine angular speed
ζ; n = Hill equation calibrating coefficients

References

1. Heywood, J.B., "Internal Combustion Engine Fundamentals," McGraw-Hill, New York, 1988.
2. Ferguson, C. and Kirkpatrick, A., "Internal Combustion Engines: Applied Thermosciences," John Wiley & Sons, Inc., New Jersey, 2016.
3. Onorati, A. and Montenegro, G., "1D and Multi-D Modeling Techniques for IC Engine Simulation," SAE International, ISBN: 978-0-7680-9352-0.
4. Heywood, J.B., "Engine combustion modeling - an overview," in: J.N. Mattavi, C.A. Amann (Eds.), Combustion Modeling in Reciprocating Engines. Plenum Press, 1978, pp. 1-35.
5. Blizard, N.C. and Keck, J. C., "Experimental and Theoretical Investigation of Turbulent Burning Model for Internal Combustion Engines," SAE Technical Paper 740191, 1974, https://doi.org/10.4271/740191.
6. Keck, J.C., Heywood, J.B., and Noske, G., "Early Flame Development and Burning Rates in Spark Ignition Engines and Their Cyclic Variability," SAE Technical Paper 870164, 1987, https://doi.org/10.4271/870164.
7. Tabaczynski, R., Ferguson, C., and Radhakrishnan, K., "A Turbulent Entrainment Model for Spark-Ignition Engine Combustion," SAE Technical Paper 770647, 1977, https://doi.org/10.4271/770647.
8. Wiebe, I. I., "Semi-empirical expression for combustion rate in engines," In Proceedings of Conference on Piston engines, USSR, 1956, pp. 185–191. (Academy of Sciences, Moscow).
9. Ghojel, J., "Review of the development and applications of the Wiebe function: A tribute to the contribution of Ivan Wiebe to engine research," *International Journal of Engine Research* 11, no. 4 (2010), 297-312, DOI: 10.1243/14680874JER06510.

10. Yeliana, Y., Cooney, C., Worm, J., Michalek, D.J., and Naber, J.D., “Estimation of double-Wiebe function parameters using least square method for burn durations of ethanol-gasoline blends in spark ignition engine over variable compression ratios and EGR levels,” *Applied Thermal Engineering* 31, no. 14–15 (2011), 2213-2220, https://doi.org/10.1016/j.applthermaleng.2011.01.040.
11. Calabrese, E.J., “Dose–Response Relationship,” Editor(s): Philip Wexler, Encyclopedia of Toxicology (Third Edition), Academic Press, 2014, 224-226, https://doi.org/10.1016/B978-0-12-386454-3.00991-X.
12. Hill, A. V., "The possible effects of the aggregation of the molecules of hemoglobin on its dissociation curves". The Journal of Physiology 40, suppl. (1910), i–vii, doi:10.1113/jphysiol.1910.sp001386.
13. Pipitone, E., Beccari, S., and Genchi, G., “Supercharging the Double-Fueled Spark Ignition Engine: Performance and Efficiency”, J. Eng. Gas Turbines Power 139, no. 10 (2017), doi: 10.1115/1.4036514
14. Rassweiler, G. and Withrow, L., "Motion Pictures of Engine Flames Correlated with Pressure Cards," SAE Technical Paper 380139, 1938, https://doi.org/10.4271/380139.
15. Gillespie, L., Lawes, M., Sheppard, C., and Woolley, R., "Aspects of Laminar and Turbulent Burning Velocity Relevant to SI Engines," SAE Technical Paper 2000-01-0192, 2000, https://doi.org/10.4271/2000-01-0192.
16. NIST-JANAF, “Thermochemical Tables, Fourth Edition,” *Journal of Physical and Chemical Reference Data*, M.W. Chase JR, 1998.
17. Woschni, G., "A Universally Applicable Equation for the Instantaneous Heat Transfer Coefficient in the Internal Combustion Engine," SAE Technical Paper 670931, 1967, https://doi.org/10.4271/670931.
18. www.ni.com